Flexible Meta-Signal Tracking: Architecture Robustness in Challenging PNT Scenarios

Flexible Meta-Signal Tracking: Architecture Robustness in Challenging PNT Scenarios

ANDREA NARDIN, Graduate student member, IEEE
Politecnico di Torino, Turin, TO 10124, Italy

FABIO DOVIS, Member, IEEE
Politecnico di Torino, Turin, TO 10124, Italy

FRANCESCA ZANIER
European Space Agency, Noordwijk, AZ 2201, Netherlands

FLOOR MELMAN
European Space Agency, Noordwijk, AZ 2201, Netherlands

***Abstract*— The idea of multichannel tracking is generally found in the Global Navigation Satellite System (GNSS) literature with a wideband approach. We further developed the concept to separately process two narrowband channels that are later combined in a dedicated delay-locked loop (DLL) in a virtual wideband fashion. To suit prospect evolution of positioning, navigation, and timing (PNT) technologies and GNSSs, we generalized the so-called meta-signal construction to the combination of components transmitted over the same bandwidth, thus expanding the range of candidate multichannel components and fostering efficient bandwidth exploitation and increased resiliency to harsh Doppler. These improvements are sustained by additional complexity at the receiver, whose robustness must be carefully assessed. The resulting architecture performance in presence of multipath and tracking noise is therefore characterized under the challenging conditions of modern GNSSs, focusing on a low earth orbit (LEO) PNT scenario. The technique can successfully bear the representative Doppler profiles and C/N_0 levels of the addressed scenarios achieving a large estimation noise reduction, even under challenging multipath conditions.**

***Index Terms*— GNSS, multichannel, meta-signals, LEO PNT, satellite navigation.**

This paragraph of the first footnote will contain the date on which you submitted your paper for review, which is populated by IEEE."This work was supported in part by the U.S. Department of Commerce under Grant BS123456." The name of the corresponding author appears after the financial information, e.g. *(Corresponding author: A. Nardin)*. Here you may also indicate if authors contributed equally or if there are co-first authors.

Andrea Nardin and Fabio Dovis are with Politecnico di Torino, Turin, TO 10124, Italy (e-mail: name.surname@polito.it). Francesca Zanier and Floor Melman are with the European Space Agency, Noordwijk, AZ 2201, Netherlands (e-mail: e-mail: name.surname@esa.int).

Color versions of one or more of the figures in this article are available online at http://ieeexplore.ieee.org.

I. INTRODUCTION

IN addition to earth-based navigation, positioning, navigation, and timing (PNT) services are already exploited in a plethora of applications [1]. Among these, precision agriculture [2], vehicle and inter-personal ranging [3], [4], [5], communication networks [6], or space applications [7], [8], [9], to name a few. However, as the range of applications expands, providing an adequate PNT service is becoming more challenging and, nevertheless, an increasing number of current and envisioned applications demands a precise and reliable PNT system [1]. In the framework of Global Navigation Satellite Systems (GNSSs) and more generally radio navigation systems (RNSs), several approaches are exploited or have been proposed to fulfill this requirement, either on the signal design side [10], [11] or through innovative processing architectures [12], [13], [14].

Among these solutions, the availability of synchronous channels can be exploited to increase the precision and the robustness of the position estimate through a *multichannel* approach, implemented within the processing chain of a receiver. A satellite constellation that offers multiple PNT services or data/pilot channels may indeed transmit more than one signal component per satellite vehicle and these components are generally synchronous to some extent, especially if they undergo the same transmission chain (frequency up-converter, amplifier chain, and antenna) [15], [16] when multiplexed together. Multiple channels availability is already a reality for GNSSs [17] and some degree of service multiplicity will be likely accommodated also by the next generation of alternative and complementary PNT technologies [18], [19], [20], [21], [14], [22], [23].

The coherency among these signals can be exploited to improve the quality of the information that is going to be extracted from them. Referring to a classical GNSS receiver architecture [24], the coherent transmission of direct sequence spread spectrum (DSSS) signal components allows a coherent multichannel *tracking*, thus merging the information content of signals at an early stage of the signal processing chain [15], [16], [25], [26], [27], [28]. As a result, the multichannel approach efficiently exploits, at a tracking level, the availability of multiple signal components to address more accurate and precise navigation solutions, while improving robustness to common impairments such as multipath and interference [29]. A single signal composed by synchronous GNSS channels received at different frequencies has been regarded as *meta-signal* [30], [31], [32], [33]. In recent years, the use of meta-signals processed as a single wideband signal has been investigated as a promising approach to effectively take advantage of multiple channels availability and extract high-quality measurements to improve positioning accuracy [34], [35], [33], [32], [36], [37].

Meta-signals however, as well as split-spectrum modulations, are generally characterized by a multi-peaked autocorrelation function (ACF) [38]. A characteristic that

might lead to false locking and biased measurements, especially when multipath is present. Such aspect must be therefore addressed in working implementations, adopting a *peak ambiguity resolution* strategy. Nonetheless, an efficient exploitation of the many available signals is limited to the combination of those signal components that are transmitted over different frequencies. Indeed, in modern GNSSs, signal components might be transmitted over the same bandwidth, carried by in-phase and quadrature carriers (e.g. Galileo E5a-I and E5a-Q) or orthogonal pseudorandom codes (e.g. E1B and E1C) [39]. In addition, the construction of such wideband meta-signals might not suit the prospect evolutions of PNT technologies and GNSSs, such as low earth orbit (LEO) PNT systems [19], [40], [41], [14], where payload are designed for rapid reconfiguration and signal components might be sharing the same bandwidth [41]. Nonetheless, signals transmitted by LEO satellites are received on Earth after experiencing severe Doppler shifts, a major cause of distortion for wideband signals.

To overcome these limitations, we generalize the meta-signal construction to the combination of signal components transmitted over the same bandwidth, thus expanding the multichannel approach to other forms of signal orthogonality, other than frequency separation [42], [14], [22]. This flexible approach can be adapted to dynamic payloads and signals configurations. Moreover, it fosters an efficient bandwidth exploitation, resulting in the use of narrower bandwidths and an increased resiliency to harsh Doppler [14], but its robustness in challenging scenarios must be carefully investigated. Indeed, the performance improvements brought in by this approach are generally sustained by an additional complexity at the receiver side, which, if not carefully addressed, can easily undermine its robustness, especially in harsh environments and modern GNSS scenarios. An implementation of this concept was preliminary investigated in [42], [14], [22] and dubbed *virtual wideband (VWB) tracking*. This original architecture has been improved to attain a more robust ambiguity resolution and better cope with multipath-induced biases. Nevertheless, a comprehensive characterization of its performance in modern challenging scenarios has never been addressed.

The objective of this work is therefore twofold. On the one hand, we want to deeply characterize this flexible meta-signal architecture in a LEO PNT context. On the other, we want to test the implementation's performance, focusing on its robustness and stressing the conditions that might lead to false locking. In Section II, a description of the proposed implementation is followed by the ambiguity resolution strategy adopted. The behavior of the proposed method in challenging conditions is then assessed in a relevant LEO PNT scenario. A detailed performance analysis is provided addressing, in particular, (*i*) the multipath impact and the associated risk of false locking, and (*ii*) the robustness of the architecture to tracking noise. The study logic behind experimental campaigns (*i-ii*) is outlined in Section III, while the resulting outcomes are provided in Section IV. Conclusions are drawn in Section V.

II. VIRTUAL WIDEBAND META-SIGNAL AND TWO-STEP PEAK DISCRIMINATION

A. Meta-Signal Rationale

The meta-signal concept introduced in [30] is based on the well-known Cramér-Rao bound (CRB) that limits the minimum achievable propagation time estimator variance σ_τ^2 such that [43]

$$\sigma_\tau^2 \geq \frac{1}{8\pi^2 \eta \beta^2} = \frac{1}{8\pi^2 \frac{C}{N_0} T \beta^2} \tag{1}$$

where

$$\beta^2 \triangleq \frac{\int_{-\infty}^{+\infty} f^2 |X(f)|^2}{\int_{-\infty}^{+\infty} |X(f))|^2} \tag{2}$$

is the square of the so-called Gabor bandwidth (GB). In the equation, the dependency on the signal-to-noise ratio (SNR) $\eta = \frac{C}{N_0} T$ is highlighted [38], [44] where T is the observation time and $\frac{C}{N_0}$ is the *carrier-to-noise-density ratio (C/N_0)*. The GB in (2) depends on the spectrum $X(f)$, which is the Fourier transform of the baseband noiseless observed signal $x(t)$ [43], [44].

It is clear that the CRB of the propagation time estimator can be reduced by increasing the GB. The net effect is to achieve, in turn, an improved position estimation in those RNSs based on time of arrival (TOA). In the GNSS literature, in the past years, several solutions have been proposed to achieve a larger Gabor bandwidth. The methods differ from the way in which the increase of the Gabor bandwidth is obtained. The straightforward, well-known, way, is the use of wider bandwidth signals, thus occupying a wider range of the frequency axis. However, in recent years, it has been proposed to achieve better resolution by processing "all together" several, narrowband, GNSS channels, received over different carrier frequencies. This approach has been referred in general as the use of GNSS *meta-signals*.

B. Generalized meta-signal model

Let us consider a set of N signals $s_i(t)$ with $i = 1, ..., N$, merged together into the signal $x(t)$, processed by a TOA estimator. According to (1), it is desirable to have a signal $x(t)$ with a large Gabor bandwidth. Under a multichannel approach, this can be obtained if the processed channel components are spread over the spectrum of $x(t)$ such that

$$x(t) = \sum_{i=1}^{N} s_i(t) e^{j2\pi f_i t} \tag{3}$$

has a large part of its energy located at the spectrum edges. An approximation of (3) can be easily obtained as a complex baseband of a received Radio Frequency (RF) signal, if the relative frequency separation among the

signal components within $x(t)$ matches the frequency separation among the components in the transmitted signal at RF. This multichannel composite signal, processed as a single signal, is known as *meta-signal* (here generalized to N signals). Nevertheless, if each signal $s_i(t)$ can be separately processed by a receiver, a composite signal whose complex baseband has the form in (3) can be effectively obtained within the receiver processing chain by modulating each carrier at f_i with the i-th signal component $s_i(t)$. The net result is still a large Gabor bandwidth signal that enters a TOA estimator. It is worth stressing that this approach can work as long as signal components can be independently processed, i.e. as they are orthogonal signals. As a result, this generalized meta-signal construction can be extended also to components transmitted over the same bandwidth, e.g. by means of in-phase and quadrature carriers or orthogonal spreading codes.

Commonplace TOA estimators are implemented through correlators. The correlation properties of a signal $x(t)$ are well-described by its ACF, defined as

$$R_{xx}(\tau) = \int_{-\infty}^{+\infty} x(t+\tau)x^*(t)\,\mathrm{d}t \ . \tag{4}$$

A signal with a large Gabor bandwidth shows a narrow main peak, a property that is indeed related to a good code-tracking performance, i.e. to an accurate TOA estimation [45]. Nevertheless, it can be proved [46] that the ACF of a meta-signal, as defined in (3), can be approximated by the sum of the ACF of its component signals modulating complex exponentials [31]. In other words,

$$R_{xx}(\tau) \approx \sum_{i=1}^{N} R_{x_i x_i}(\tau) = \sum_{i=1}^{N} R_{s_i s_i}(\tau) e^{j2\pi f_i \tau} \ , \tag{5}$$

where $x_i(t) = s_i(t)e^{j2\pi f_i t}$. Note that the approximation in (5) becomes an equality when the signals $s_i(t)$ are confined to disjoint bandwidths.

C. Virtual Wideband architecture

The generalization of the meta-signal concept to other forms of signal orthogonality motivated the development of a tracking architecture that can, on the one hand, process a multichannel signal whose complex baseband representation has the form in (3) and, on the other, drive the generation of each f_i carrier in a closed-loop fashion. The block scheme in Fig. 1 illustrates such architecture.

Without loss of generalization, the scheme describes a tracking stage for $N = 2$ channels. Two received intermediate frequency (IF) signals, $y_{1,\mathrm{IF}}(t)$ and $y_{2,\mathrm{IF}}(t)$, undergo through the two co-dependent loops for carrier and code wipe-off, typical of a GNSS receiver's tracking stage [17]. Then, before entering in a multichannel DLL, a local numerically-controlled oscillator (NCO), driven by the DLL, is used to obtain the desired frequency separation f_m between the processed components.

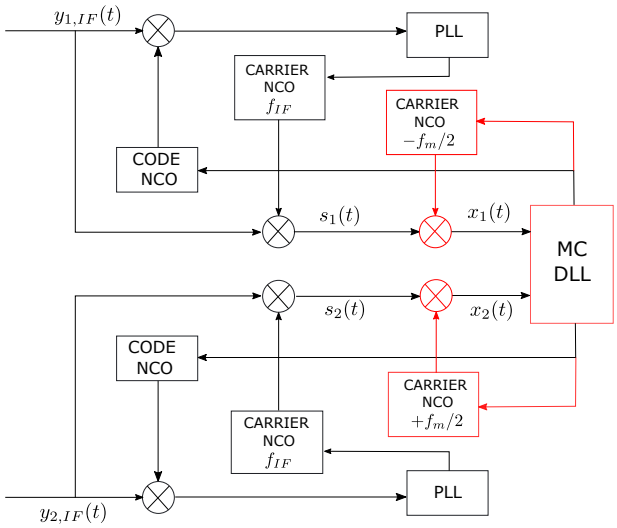

Fig. 1: Virtual Wideband tracking implementation (second step). Distinctive blocks highlighted in red.

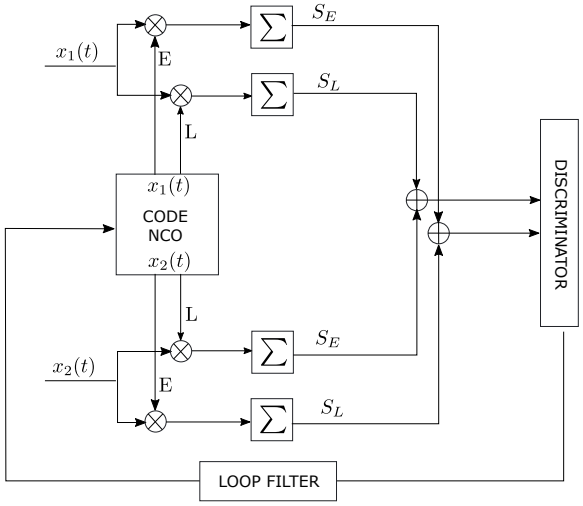

Fig. 2: Multichannel delay-locked loop (DLL) implementation.

Inside the DLL (Fig. 2), the two channels are combined at a post correlation level, exploiting the property in (5) and thus merging the correlators outputs instead of the meta-signal components. In the proposed scheme, a classical *early-late* (E-L) architecture is used [24]. It is worth highlighting the introduction of a single loop filter and a single code NCO in the multichannel (MC) DLL. These originally separated blocks [42], [22] are now merged to reduce the independence of the interconnected loops of the two channels, thus providing a more robust estimation. The discriminator behavior can be described by the so-called *S-curve*, a nominal characteristic function that depends on signals' ACF and the discriminator function and relates the discriminator output with the local replicas shift in the correlators [17].

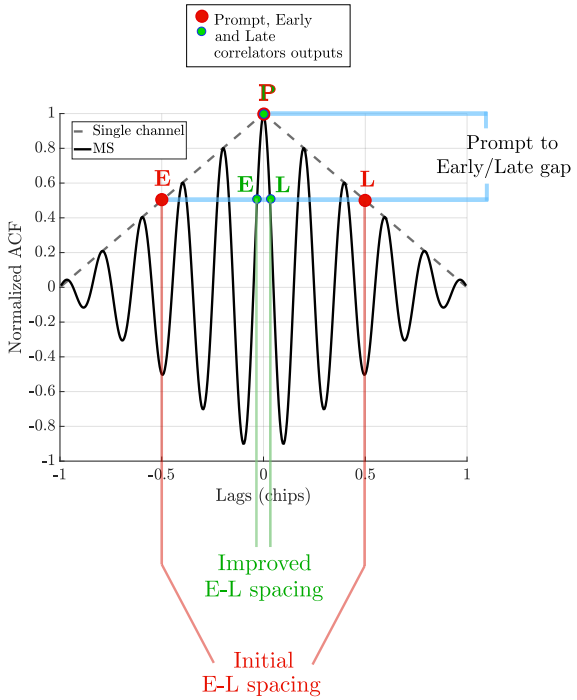

Fig. 3: ACF of a single BPSK(1) signal and a meta-signal made by two BPSK(1) channels.

D. Ambiguity resolution and false locking

A major problem with meta-signals is that they exhibit a multi-peaked ACF (see Fig. 3 as an example with two signal components). Therefore, at low SNR, side peaks can rise above the main peak leading to false locking and in turn to a biased TOA estimation, a well-known problem for narrowband signals [47], [48]. This means that, if we can cope with the ambiguity, it is possible to leverage the increased sharpness to reduce the correlator Early-minus-Late (E-L) spacing, while keeping the same gap between Prompt (P) and Early (E) or Late (L) correlator outputs (see Fig. 3). As a consequence, we can tolerate the same amount of noise (thanks to the gap) while obtaining a reduced code tracking jitter (thanks to the E-L spacing reduction) [24].

The number of peaks and, therefore, the severeness of the ambiguity depends on the frequency separation between the combined channels. Hence, a working tracking stage implementation should overcome the peak ambiguity through suitable techniques. This can be achieved, for instance, by resorting to ambiguity resolution methods developed for high-order Binary Offset Carrier (BOC) modulations [49], [50] or by implementing a *two-step* processing of the composite signal, where, during an initial step, each signal component is tracked independently allowing the correlators to align unambiguously on the main peak [31]. Indeed, the inherent flexibility of the multichannel approach allows to seamlessly move from a single channel (SC) step, where a plain tracking stage is used, to a MC step, when the architecture in Fig. 1 is adopted. After an initial SC tracking, the MC processing is triggered based on a locking condition, which might be based on a phase lock indicator (PLI) [51], defined as

$$\mathrm{PLI} = \frac{I_P^2 - Q_P^2}{I_P^2 + Q_P^2} \tag{6}$$

where I_P and Q_P are, respectively, the in-phase and quadrature phase prompt correlator outputs [17], computed at each tracking loop iteration. The MC stage is then enabled when the PLI is above a given threshold, defined as a receiver parameter. It is worth remarking that the use of a lock detector during the SC step is an essential part of the proposed architecture, as it enables a profitable MC stage. Its observation in subsequent stages is not vital to a working implementation, but could be exploited as a performance indicator.

A high-level overview of these sequential stages is provided by Fig. 4. Notice that a *σ-aware channel selector* has been employed to obtain a more robust transition between the SC and MC step. This block allows to select which of the N SC tracking output flows will be used to initialize the MC code NCO and DLL loop filter blocks. This selection is based on the statistical characteristics of the filtered discriminator output, as estimated by each SC tracking stage. In particular, the channel that exhibits the lower variance, estimated over a window of accumulated observations, is selected to initialize the subsequent MC stage. The selector has been introduced with respect to previous designs [42], [22] to prioritize the channel characterized by a potentially more robust estimation, while taking advantage of the channel diversity.

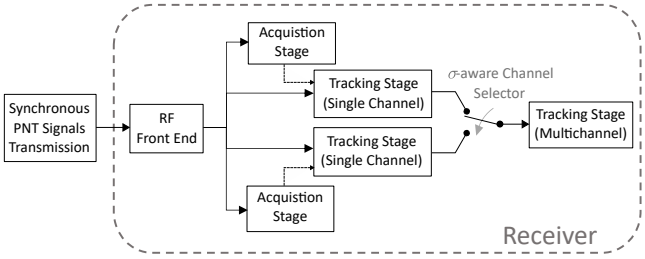

Fig. 4: End-to-end system architecture using a two-step ambiguity resolution method. Example with $N = 2$ channels.

III. STUDY LOGIC

A detailed characterization of the architecture was pursued through an experimental campaign, carried out with the scope of characterizing the implementation's robustness under challenging conditions. The results of this experimental campaign are provided in Section IV. We investigated in particular:

(*i*) the technique's behaviour under unfavourable multipath (MP) conditions associated with high risk of false locking (Section IV-A);
(*ii*) the technique's robustness to larger DLL noise bandwidths, exploring its behavior with respect to the

amount of noise that can be tolerated in the tracking loop (Section IV-B).

The performance analysis was performed with respect to a target LEO PNT scenario, assuming transmitted signal waveforms that are known to the receiver. The investigation of a signals-of-opportunity approach of the proposed method is out of the scope of this work [52]. To process realistic LEO PNT signals, a PNT receiver must be fed with signals characterized by Doppler profiles which are consistent with the reference LEO constellation. A constellation propagator tool (AGI STK) was used to simulate the LEO satellites and to model the communication channel. After selecting a user location on Earth, we were able to extract the frequency shift experienced by the receiver on Earth during the satellite passage due to the Doppler effect. Despite the potentially higher received power that should characterize LEO PNT frameworks [20], a more conservative choice of C/N_0 levels allows to stress the implementation robustness while targeting power levels closer to the usual medium earth orbit (MEO) GNSS range. The C/N_0 and the Doppler profile were used to feed a binary signal generator. The signal generator outputs two signals consistent with the Doppler profile and the C/N_0 level provided. These signals are then combined in a multi-channel fashion within the tracking stage of a software receiver. An overview of the simulation blocks is provided in Fig. 5.

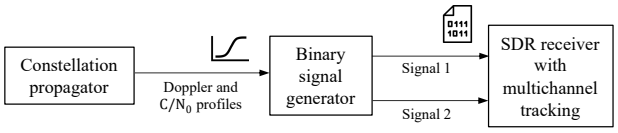

Fig. 5: Simulation blocks.

A general view of the parameters configuration of the test campaigns is reported in Table I. The values in the domain of "orbital parameters", "transmitter parameters", "atmospheric impairments", and "user conditions" were used to model the LEO constellation simulator block in Fig. 5. An altitude of 1200 km was set to target a realistic LEO PNT scenario, inspired by OneWeb [53] and Starlink [54] constellations. The values reported in the "signal generator" domain were used to setup the signal simulator for the generation of binary samples and those relative to "receiver configuration" were set to properly tune the software receiver to process the generated digital signals. The signals involved in the simulations are BPSK(1) signals with the same modulation characteristics of the Global Positioning System (GPS) C/A signal. Due its linearity and simplicity, BPSK is especially suitable for time-based positioning and a common choice in the PNT context [19]. Furthermore, besides their relevance, the choice of using basic PNT signals is motivated by the goal of not adding additional complexity to the receiver implementation, steering our attention on the proposed technique robustness in a baseline implementation. However, it is important to remark that, in principle, any heterogeneous set of known waveforms can be tracked through a VWB architecture, though one must carefully consider the resulting complexity burden during MC processing.

Two different satellite passages were analyzed to offer two different Doppler scenarios. A low elevation peak (LEP) passage with mild Doppler conditions and a lower average C/N_0; and a passage above the zenith, namely high elevation peak (HEP) passage, subject to intense Doppler conditions, a generally non-linear Doppler profile, and a higher average C/N_0. The characteristics of these trajectories depends on the constellation configuration in Table I and each test is repeated for the two satellite passage profiles. The resulting Doppler frequency shifts along time are shown in Fig. 6 and the configurations for these two scenarios are reported in Table II.

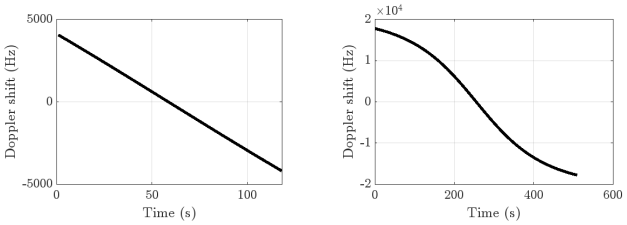

(a) LEP passage. (b) HEP passage.

Fig. 6: Doppler shift for different satellite passages.

A snapshot of the simulated scenario in the LEO constellation propagator software (AGI STK) is reported in Fig. 7. In the proposed frame, the satellite is at the zenith with respect to the user.

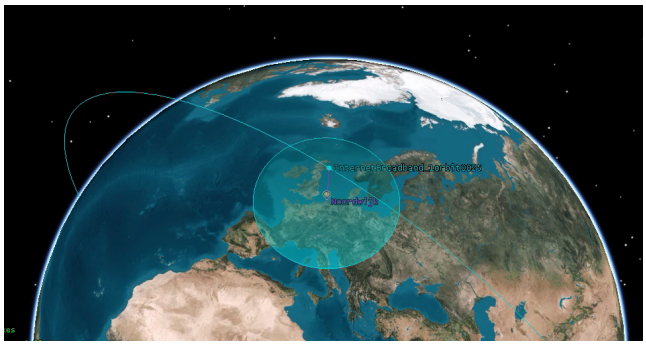

Fig. 7: Simulated scenario. High elevation satellite passage example.

The main performance metric is the code estimation error, measured as the output of the DLL discriminator extracted within the receiver's tracking stage. This metric will be referred to as *discriminator output* and measured in chips. The two-step approach allows to compare a SC output of a plain tracking stage (first step) with the result from MC processing (second step, Fig. 1). The performance can be then discussed by comparing

TABLE I: Common configuration for the experiments.

Domain	Parameter	Value
Orbital Parameters	Inclination	51.9°
	Altitude	1200 km
Transmitter parameters	Modulation	BPSK(1)
	DSSS code length	1023
	Data rate	50 bit/s
	CDMA spread	20460 chips/bit
	Bandwidth	2.046 MHz
	Carrier frequency	1062 MHz (L band)
	Edge of coverage	30°
Atmospheric impairments	Cloud and Fog model	ITU-R P840-6
	Tropospheric scintillation	ITU-R P618-12
	Ionospheric fading	ITU-R P531-13
User conditions	User Location	Noordwijk (52.24°,4.45°)
Signal generator	Sampling frequency	25 MHz
	IF	0 Hz
	Code delay	0.5 ms
	Binary signal type	int8
	Quantization bits	7
	Antenna gain	0 dBi
Receiver configuration	PLL order	3
	SC E-L spacing	1 chip
	MC E-L spacing	0.025 chip
	PLI threshold	0.8
	Virtual frequency separation (f_{m})	18.414 MHz
	Coherent integration time	1 ms
	DLL noise bandwidth	20 Hz
	PLL noise bandwidth	40 Hz

TABLE II: Scenario characterization.

Doppler profile	Average C/N_0 (dB-Hz)	Average power[a] (dBW)	Passage duration (s)
LEP	40.0	-158.0	117
HEP	50.0	-149.0	509

[a]Carrier isotropic power.

the steady-state condition of the code estimation error in the two cases. The standard deviation (STD) of the discriminator output, σ_d, will be estimated (in meters) and used as an aggregated metric for ease of comparison among the experiments. The standard deviation will be computed separately over the SC processing stage and the MC processing stage.

Notice that the MC triggering condition was forced to be activated only after a certain amount of time. This means that the condition of having PLI value above the threshold is not considered until a certain number of tracking iterations (corresponding to 20 s). This allows the SC stage to last longer in order to provide sufficient data for statistical characterization of the discriminator output. Furthermore, a transient of about 1 s was noticed across all the tests. Consequently, an initial portion of 2 s is left out from the statistical analysis to accommodate the transient with some margin and avoid the latter causing degraded observations.

During the experiments, the output of the loop filter acting on the discriminator output (Fig. 2) was monitored as well. This quantity, used to steer the code NCO, can be converted to a measure of the code rate and is susceptible to line of sight (LOS) dynamic stress, such as Doppler effects. To remove the Doppler dependency, we employed a quasi-noiseless signal—a LOS signal simulated at a very high C/N_0 of 100 dB-Hz adopted as a reference. The code rate estimate obtained in a SC tracking loop from this signal was subtracted from the MC code rate estimate under test. The resulting metric is reported to complement the performance analysis providing an accurate measure of the estimated *code-rate error*. This not only enables observation of the estimation error with respect to a ground truth reference but also allows the detection of biased estimation processes.

Indeed, as described in Section II D, this meta-signal approach introduces peak ambiguity in the ACF, potentially causing false-locking in the tracking, especially for signals impaired by MP. At each tracking loop iteration, the code rate estimate observed with the 100 dB-Hz LOS signal should differ with respect to what measured with MP signals because of noise and possibly due to the presence of MP itself. However, on average, the difference of the two estimates, i.e. the code-rate error, should approach zero if the code rate estimation under MP is unbiased. Such monitoring of the estimation bias simulates the presence of a robust peak ambiguity resolution block, which could be implemented by resorting to well-established methods reported in literature [49]. Although the outcomes of code-rate error averages are omitted for brevity, false locking monitoring was conducted for each set of

experiments in Section IV, and no bias was detected. This successful validation of the two-step ambiguity resolution strategy, carried out in specifically-designed challenging MP scenarios ensures the effectiveness of the approach under worst-case conditions, as explained in the next section. The subsequent sections, offer a more in-depth description of the study logic that guided the experiments for assessing the technique's performance (*i*)-(*ii*).

A. Performance under challenging multipath conditions

The multipath tests are intended to challenge the receiver, inducing the conditions that are likely to trick the tracking stage to lock on a false locking point. The selected MP model is a two-ray propagation model. The analysis is carried on using a specific narrow correlator (non-coherent E-L power normalized [55]), suitable to an effective false-lock mitigation. To this end, two different reflected signal (RS) amplitudes were selected, thus referring to as many diagrams, representing multipath errors induced by in-phase and antiphase reflection, as shown in Fig. 8. Four different RS delays are ultimately selected for each of the plots, which are therefore "sampled" at the corresponding delays, choosing those values that are relevant for the locking robustness test. In particular, both for in-phase and anti-phase RSs, the delays that give the maximum and minimum S-curve bias were selected (see the green circles in Fig. 8). The resulting values depends on the virtual frequency separation between channels (18.414 MHz), the type of discrimination function (non-coherent E-L power normalized [55]) and the discriminator spacing (0.025 chips). The RS is present for the full duration of the tests, that is, for both the SC and MC stages.

To complement the multipath characterization, an additional set of experiments was performed under a realistic multipath model (Test 17 and 18). The simulated deterministic model was generated by modeling buildings and streets in a realistic urban scenario. At each instant, the position of the satellite and the user are considered, and the multi-ray propagation is computed based on the geometry and characteristics of the surfaces. The scattering model is based on radar cross sections [56] while the ground reflections are simulated through Snell's law [57]. The resulting propagation environment is a multi-ray model with short-lifespan reflections in an urban scenario. Additionally, vehicular dynamics are simulated by specifying a user trajectory at constant speed. Table III summarizes the MP signal characteristics for each test.

B. Robustness with respect to DLL noise bandwidth

The proposed VWB architecture was tested with respect to the amount of noise that the MC tracking loop can sustain. Two different Doppler profiles and C/N_0 levels were simulated as described by the LEP and HEP scenarios (see Table II). The MP configuration of Test 1 and Test 9 from Table III are selected to perform the tests in representative challenging MP conditions for, respectively, LEP and HEP scenarios. The aim is to stress the receiver within realistic conditions but varying the DLL noise bandwidth. Two different values of the DLL noise bandwidth were chosen arbitrarily, changing the previous working conditions of the DLL by increasing the loop bandwidth up to one order of magnitude. The receiver configuration characteristics that drove the test campaign are summarized in Table IV.

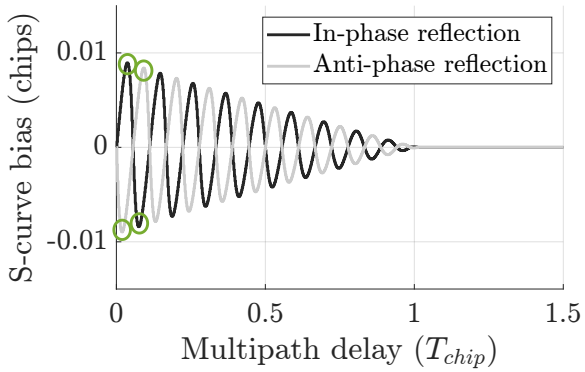

(a) Signal-to-multipath ratio (SMR) = 6 dB.

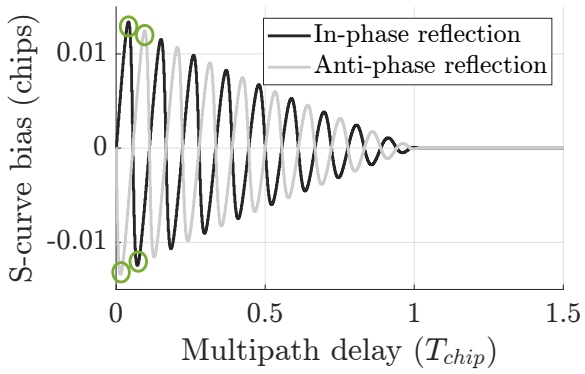

(b) SMR = 3 dB.

Fig. 8: Multipath errors induced by in-phase and antiphase reflection using a non-coherent E-L power normalized discriminator [24]. 2 BPSK(1) channels, virtual freq. separation 18.414 MHz, spacing = 0.025 chips.

IV. RESULTS

In this section we present the results from the experimental campaign. A comprehensive discussion on the investigation outcomes under different conditions is provided, according to the tested scenarios defined in Section III.

A. Performance under challenging multipath conditions

The examination of the DLL observables was performed for the two reference Doppler profiles scenarios

This article has been accepted for publication in IEEE Transactions on Aerospace and Electronic Systems. This is the author's version which has not been fully edited and content may change prior to final publication. Citation information: DOI 10.1109/TAES.2024.3359594

TABLE III: Test-dependent settings.

Test no.	Doppler profile	SMR (dB)	RS phase (rad)	RS delay (chips)
1	LEP	3	0	0.0418[a]
2	LEP	3	π	0.0141[b]
3	LEP	3	0	0.0717
4	LEP	3	π	0.0957
5	LEP	6	0	0.0365
6	LEP	6	π	0.019
7	LEP	6	0	0.0745
8	LEP	6	π	0.092
9	HEP	3	0	0.0418
10	HEP	3	π	0.0141
11	HEP	3	0	0.0717
12	HEP	3	π	0.0957
13	HEP	6	0	0.0365
14	HEP	6	π	0.019
15	HEP	6	0	0.0745
16	HEP	6	π	0.092
17	LEP	5–35	0–2π	0.002–0.512
18	HEP	5–35	0–2π	0.002–0.512

[a]Maximum S-curve bias.
[b]Minimum S-curve bias.

TABLE IV: Tested receiver configurations.

Test no.	Doppler profile	DLL noise bandwidth (Hz)
1	LEP	150
2	LEP	250
3	HEP	150
4	HEP	250

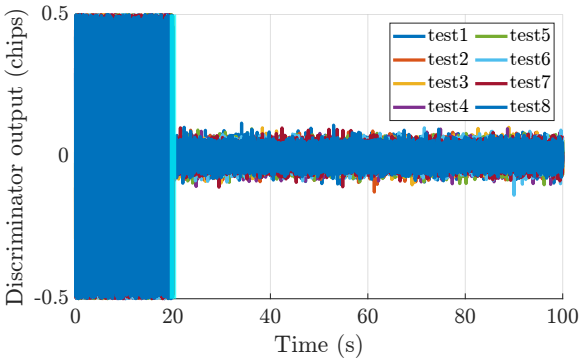

(a) LEP satellite passage.

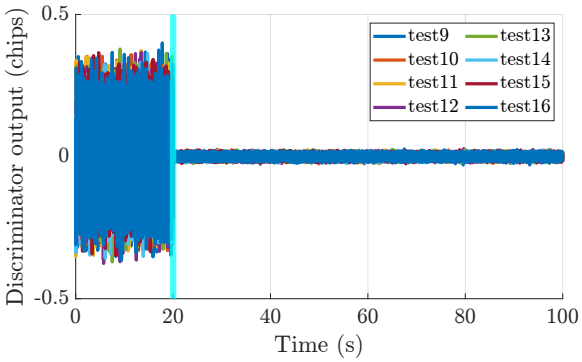

(b) HEP satellite passage.

Fig. 9: Discriminator output of MP-affected signals. The cyan vertical line marks the beginning of the MC processing stage. Only the first 100 s are shown.

of Fig. 6 (LEP and HEP). In each test the signals are impaired by a different multipath condition. However, each of the two satellite passages has a constant duration for the Earth-located user, favoring the aggregation of the test data by satellite passage scenario.

Focusing on the LEP scenario, the time series of discriminator output and code-rate error are reported in Fig. 9a and 10a respectively, where the results from Tests 1-8 are superimposed. In the figure, a clear reduction of the code tracking noise is visible once the MC processing is activated (highlighted by the cyan vertical line). At a first glance, the outcomes of the tracking loops have the same behavior under all the different MP scenarios. This should come as no surprise since according to Fig. 8, the MP characteristics are almost equally challenging. The multipath-induced errors cause indeed a set of S-curve bias values of the same order of magnitude for the selected RS configurations. The results of Fig. 9 have been aggregated for an easier comparison and reported in Table V. The STD of the discriminator output (σ_d) is computed both over the SC and the MC processing outcomes (first and second step). Comparing the two set of values it is possible to observe that a less noisy discriminator output through SC processing corresponds to a low noise estimation through MC combining. The two sets have therefore similar trends. However, their magnitudes are much more different. In fact, as highlighted by the last row of Table V, the STD reduction produced by the MC stage is always more than 90 % for all the tests and σ_d is reduced by about one order of magnitude. The technique is therefore beneficial in this scenario under all the tested MP configurations.

The HEP scenario is characterized by higher Doppler levels and a non-linear Doppler profile (see Fig. 6b). However, the higher C/N_0 associated with the scenario should improve the estimation quality. Looking at the DLL metrics reported in Fig. 9b and 10b, a reduction of the estimation noise is visible with respect to the LEP scenario. This result is also confirmed by the aggregated discriminator output data of Table VI.

The outcomes derived under the dynamic multi-ray model are depicted in Fig. 11. These resultant values align closely with the previously obtained results for the two-ray scenario, as also indicated in Tables V and VI. The observation of such comparable outcomes reaffirms the advantageous trait of a high-slope multipeaked ACF in managing close-in MP scenarios [46]. Additionally, this realistic setting emphasizes the presence of generally weaker reflected rays, which have a reduced ability to disrupt a locked tracking loop.

Comparing Tables V and VI, it is clear that the higher C/N_0 of this last scenario dominates the performance with respect to the harsher Doppler conditions. A gen-

TABLE V: STD of discriminator output under challenging MP conditions. LEP satellite passage.

Test Id	1	2	3	4	5	6	7	8	17
SC estimated σ_d (m)	70.33	70.33	70.33	70.33	70.33	70.33	70.33	70.33	77.34
MC estimated σ_d (m)	5.57	5.57	5.57	5.57	5.57	5.57	5.57	5.57	5.33
σ_d reduction (%)	92.1	92.2	92.2	92.2	92.1	92.2	92.1	92.1	93.1

TABLE VI: STD of discriminator output under challenging MP conditions. HEP satellite passage.

Test Id	9	10	11	12	13	14	15	16	18
SC estimated σ_d (m)	29.31	29.31	29.31	29.31	29.31	29.31	29.31	29.31	29.54
MC estimated σ_d (m)	1.76	1.76	1.76	1.76	1.76	1.76	1.76	1.76	2.67
σ_d reduction (%)	94.3	94.3	94.3	94.3	94.3	94.2	94.2	94.2	91.0

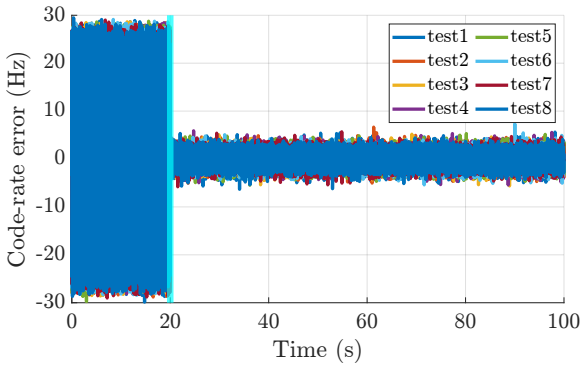

(a) LEP satellite passage.

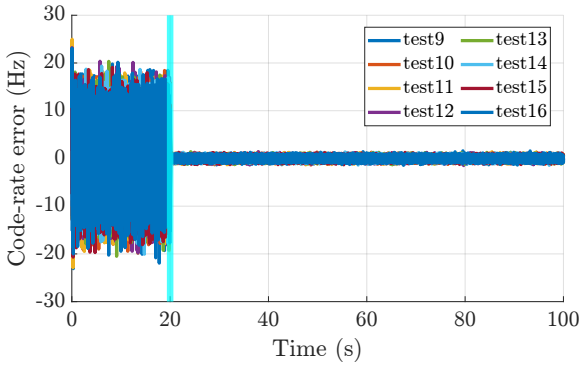

(b) HEP satellite passage.

Fig. 10: Code-rate error of MP-affected signals. The cyan vertical line marks the beginning of the MC processing stage. Only the first 100 s are shown.

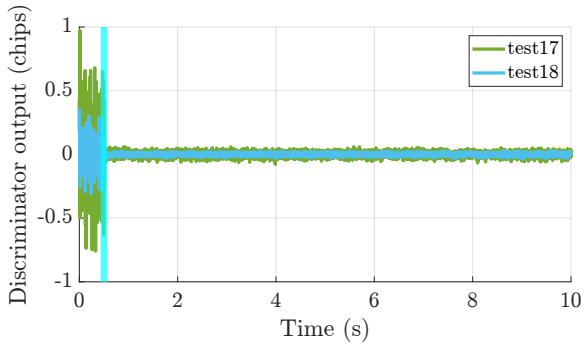

(a) Discriminator outputs.

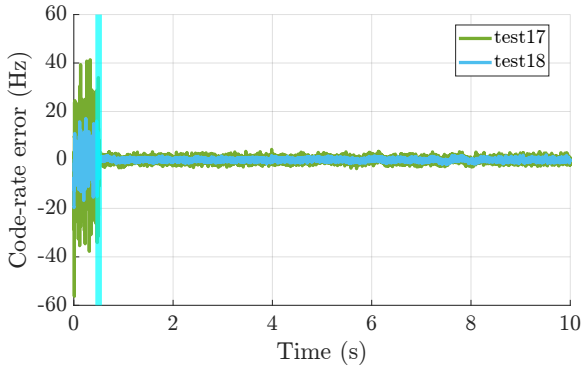

(b) Code-rate errors.

Fig. 11: DLL observables under the dynamic multi-ray model. LEP and HEP scenarios are superimposed. Due to the large computational burden, only 10 s were simulated and a0.5 s delayed MC triggering was enforced.

erally lower discriminator output noise is in fact visible both for the SC and the MC processing, where STD values move from about 29 m to less than 2 m. Nonetheless, the gain provided by the technique through σ_d reduction is comparable with the reduction in Table V. This shows that the effectiveness of the technique is not greater under such higher C/N_0 and non-linear Doppler scenario, but rather it acts on an already more accurate estimation.

B. Robustness with respect to DLL tracking noise

The capability of the proposed architecture to mitigate signals affected by MP was further challenged in the following tests to assess the potential of the VWB tracking loop to bear noise within the DLL. A set of tests has been performed according to the study logic of Section III B.

In the tested conditions, the VWB receiver can track a signal affected by MP using a DLL noise bandwidth as wide as 150 Hz. This was demonstrated in the first test of the LEP scenario (Test 1 from Table IV). Fig. 12a

reports the result of the discriminator output. In the figure, the STD of the discriminator output moves from 79.12 m during the SC stage to 5.86 m for MC processing, resulting in a STD reduction of 92 %, as reported in Table VII.

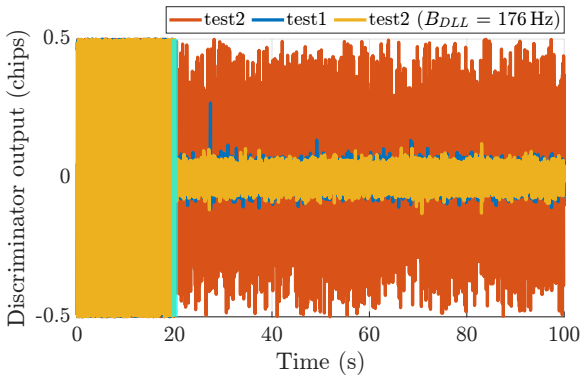

(a) LEP satellite passage.

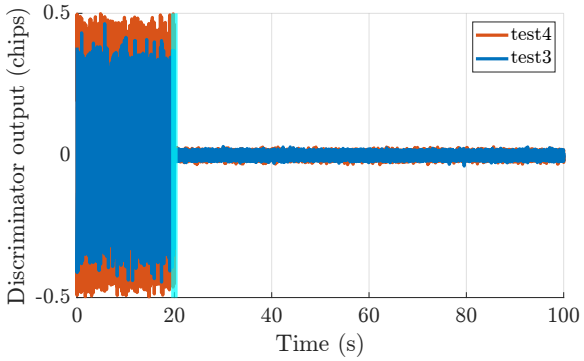

(b) HEP satellite passage.

Fig. 12: Discriminator output of MP-affected signals using different DLL noise bandwidths. Only the first 100 s are shown.

TABLE VII: STD of discriminator output. Tests under extended DLL noise bandwidth.

Doppler profile	LEP		HEP	
Test Id	Test 1	Test 2[a]	Test 3	Test 4
SC estimated σ_d (m)	79.12	82.05	41.03	64.47
MC estimated σ_d (m)	5.86	5.86	2.05	2.05
σ_d reduction (%)	92.3	92.5	95.0	96.8

[a]DLL BW = 176 Hz .

The successful tracking for this test can be confirmed by looking at the code-rate error in Fig. 13a and the main observables estimated within the tracking stage, shown in Fig. 14a. In the figure, the estimated Doppler carrier frequency matches the profile of the current scenario (Fig. 6a), the code-rate estimate (lower plot) is consistent with the profile as well and positioned around the correct values, and the values of I_P and Q_P (top plot) are correctly separated, an evidence of phase locking.

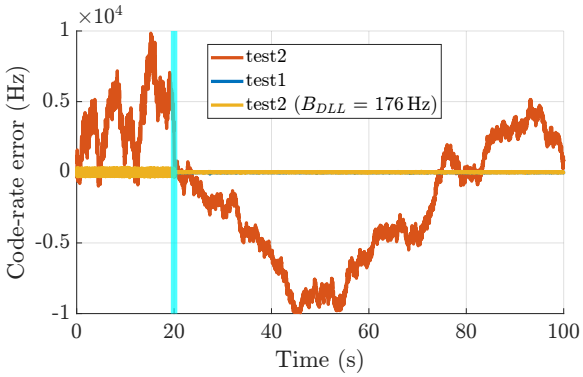

(a) LEP satellite passage.

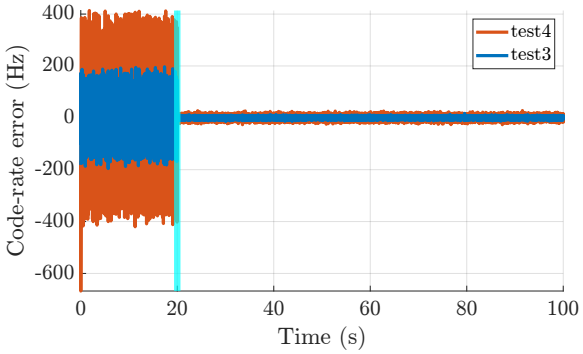

(b) HEP satellite passage.

Fig. 13: Code-rate error of MP-affected signals using different DLL noise bandwidths. Only the first 100 s are shown.

On the other hand, the same signal received using a 250 Hz DLL bandwidth as for Test 2 in Table IV cannot be tracked. This is clearly visible by inspecting the code-rate error in Fig. 13a and the outcome of the tracking stage in Fig. 14b, where the estimates are completely off-target and the I_P and Q_P components are continuously mixed. It is worth stressing however, that setting such large DLL bandwidth disrupts the performance of the plain SC receiver as well, as shown in the first 20 s of the plots in Fig. 13a and 14b. The latter shows indeed a similar behavior and it cannot track the incoming signal.

In the current scenario, the maximum DLL bandwidth that allows to successfully track the incoming signal is 176 Hz. The discriminator output and code-rate error in this configuration are also reported in Fig. 12a and 13a and the advantage provided by the technique by means of STD reduction is shown again in Table VII, where the discriminator output is reduced from around 82 m to 5.86 m.

A plain SC receiver under the same conditions can tolerate a DLL bandwidth up to 220 Hz, as shown by Fig. 14c. A multichannel DLL block is thus less robust to noise with respect to a plain DLL. However, a 176 Hz bandwidth is much higher than what is necessary to successfully track signals in the investigated scenarios (20 Hz

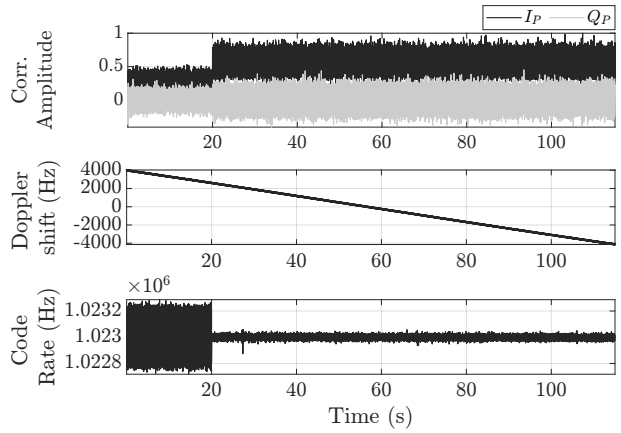

(a) Test 1 (DLL bandwidth = 150 Hz).

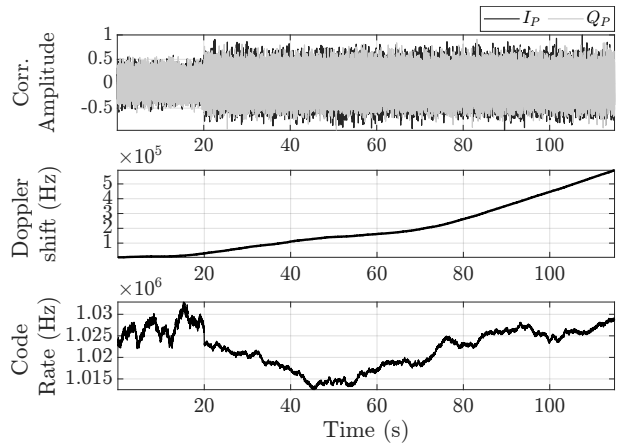

(b) Test 2 (DLL bandwidth = 250 Hz).

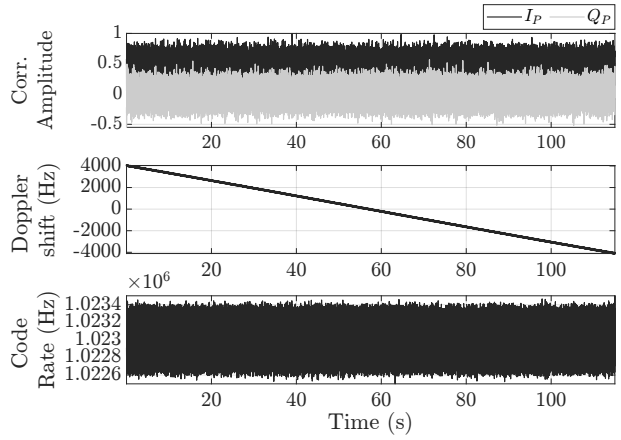

(c) Test 2 (DLL bandwidth = 220 Hz). SC receiver.

Fig. 14: Tracking loop observables for different DLL bandwidths. LEP scenario.

was set for other experiments, see Table I); therefore it can potentially enable also the tracking of signals transmitted at higher carrier frequencies.

The higher C/N_0 of the HEP scenario is again less challenging for the multichannel receiver, despite the non-linear Doppler profile of the scenario. The more favorable C/N_0 allows the VWB receiver to successfully track the signal during both HEP tests (Test 3 and Test 4), bearing a DLL bandwidth which can be as wide as 250 Hz. The benefits provided by the MC tracking in such conditions are visible in Fig. 12b and 13b and summarized in Table VII through the observation of σ_d. It is interesting to notice that the difference between the SC estimated σ_d of the two tests is larger than the LEP case. The SC estimated σ_d experienced for a reduced DLL bandwidth (Test 3) is smaller than what experienced in Test 4. However, the use of MC tracking is more effective for Test 4, resulting in two comparable performances when it is activated.

V. CONCLUSIONS

In this document a deep characterization of the VWB receiver and its performance in a LEO PNT scenario has been provided. The outcomes from these investigations allow to draw several important conclusions that are addressed in the following.

The analysis of the performance under challenging MP conditions of Section V-A demonstrated that the technique can cope with the multipath impairment in a simplified two-ray scenario. The tests performed showed a very similar response to different RS delays and amplitudes (Tables V and VI). Moreover, despite different C/N_0 and Doppler conditions a similar performance gain could be observed, with σ_d reduction that is always above 90%. The technique is therefore beneficial in a LEO PNT framework and in a scenario characterized by signals affected by moderate MP (e.g. some urban or suburban scenarios). In particular, the analysis of the HEP scenario highlighted how a higher C/N_0 is more desirable than a less-challenging Doppler profile. Thanks to the use of a narrowband approach, the proposed architecture reacts well under challenging Doppler conditions. As a result, the C/N_0 is the dominant performance driver with respect to the Doppler shift.

To test the multichannel DLL response to noise, a loop bandwidth extension has been tested in Section V-B. For a relevant extension to 150 Hz a moderate performance worsening has been observed with respect to the MP tests. To this purpose, compare Test 1 and Test 9 from Tables V and VI with Test 1 and Test 3 from Table VII, respectively. This means that the receiver can likely track higher Doppler rates, without disrupting its code estimation accuracy. It has been also observed, however, that the proposed architecture is less robust to noise than a plain SC receiver. The latter is in fact able to track a signal received at 40 dB-Hz, within the LEP scenario, using a DLL bandwidth of 220 Hz. On the other hand, a VWB receiver can correctly track the same signal using a loop as large as 176 Hz, whereas a larger bandwidth would let the noise to disrupt the tracking. Nevertheless, a 176 Hz bandwidth is a reasonable range, even for the challenging LEO PNT scenario under consideration. Furthermore, with a higher C/N_0 level, such as that in the HEP scenario, the VWB can correctly track a signal received with a 250 Hz loop

bandwidth, with a minimal performance loss with respect to a 20 Hz bandwidth (compare Test 9 of Table VI with Test 4 of Table VII). This is quite reasonable since the harsher Doppler conditions of the HEP scenario are well tolerated by the extended loop bandwidth, while the better C/N_0 ratio helps in reducing the amount of noise that enters in the loop through the widened noise bandwidth.

These results provide an insightful characterization of this multichannel technique, which has been proved adequate to successfully follow the representative Doppler profiles and C/N_0 levels of the addressed LEO PNT scenario, under moderate multipath conditions. The VWB architecture has the potential to be beneficial in the LEO PNT paradigm, at the cost of a larger complexity on the user side. Nevertheless, during the design process of the LEO PNT system, performance improvement could be obtained also in other ways, acting at signal level, thus balancing the increased complexity between system and user side.

ACKNOWLEDGMENT

This work has been developed in the framework of the activity *INNovative User receiver processing and ENhanced signals in gnss DOmain (INNUENDO)* funded by the European Space Agency (ESA). The project was carried out in the scope of investigating "Enhanced GNSS signals in space and user receiver processing" in response to ESA AO-1-9585/19/NL/CRS, Activity No. 1000023741 in the "esa-star" system, Item no. 18.1ET.29.

REFERENCES

[1] European Union Agency for the space program
EUSPA EO and GNSS market report
EUSPA, Tech. Rep., 2022.

[2] W. Wang, N. Okati, I. Tanash, T. Riihonen, and E.-S. Lohan
Location-based beamforming architecture for efficient farming applications with drones
In *2019 International Conference on Localization and GNSS (ICL-GNSS)*, 2019, pp. 1–6.

[3] A. Minetto, A. Nardin, and F. Dovis
Tight integration of GNSS measurements and GNSS-based collaborative virtual ranging
In *Proceedings of the 31st International Technical Meeting of the Satellite Division of The Institute of Navigation (ION GNSS+ 2018)*, Miami, Florida, September 2018, pp. 2399–2413.

[4] A. Minetto, A. Nardin, and F. Dovis
GNSS-only collaborative positioning among connected vehicles
In *Proceedings of the 1st ACM MobiHoc Workshop on Technologies, MOdels, and Protocols for Cooperative Connected Cars*, ser. TOP-Cars '19. New York, NY, USA: Association for Computing Machinery, 2019, p. 37–42. [Online]. Available: https://doi.org/10.1145/3331054.3331552

[5] A. Minetto, A. Nardin, and F. Dovis
Modelling and experimental assessment of inter-personal distancing based on shared gnss observables
Sensors, vol. 21, no. 8, 2021. [Online]. Available: https://www.mdpi.com/1424-8220/21/8/2588

[6] M. Pini *et al.*
Satellite-derived time for enhanced telecom networks synchronization: the root project
In *2021 IEEE 8th International Workshop on Metrology for AeroSpace (MetroAeroSpace)*, 2021, pp. 288–293.

[7] A. Minetto, F. Dovis, A. Nardin, O. Vouch, G. Impresario, and M. Musmeci
Analysis of GNSS data at the Moon for the LuGRE project
In *2022 IEEE 9th International Workshop on Metrology for AeroSpace (MetroAeroSpace)*, 2022, pp. 134–139.

[8] A. Nardin, A. Minetto, O. Vouch, M. Maiani, and F. Dovis
Snapshot acquisition of GNSS signals in space: a case study at lunar distances
In *Proceedings of the 35th International Technical Meeting of the Satellite Division of The Institute of Navigation (ION GNSS+ 2022)*, Denver, Colorado, September 2022, pp. 3603 – 3617.

[9] A. Nardin, A. Minetto, S. Guzzi, F. Dovis, L. Konitzer, and J. J. K. Parker
Snapshot tracking of GNSS signals in space: A case study at lunar distances
In *Proceedings of the 36th International Technical Meeting of the Satellite Division of The Institute of Navigation (ION GNSS+ 2023)*, Denver, Colorado, September 2023, pp. 3267–3281.

[10] R. Hirokawa, I. Fernández-Hernández, and S. Reynolds
Ppp/ppp-rtk open formats: Overview, comparison, and proposal for an interoperable message
NAVIGATION: Journal of the Institute of Navigation, vol. 68, no. 4, pp. 759–778, 2021. [Online]. Available: https://navi.ion.org/content/68/4/759

[11] X. Zhang, Z. Yao, and M. Lu
Optimizing the Gabor bandwidth of satellite navigation signals by MCS signal expression
Science China Physics, Mechanics and Astronomy, vol. 54, no. 6, pp. 1077–1082, Jun 2011.

[12] A. Emmanuele, M. Luise, F. Zanier, and M. Crisci
Selective accuracy and multiresolution capabilities are intrinsic features of multicarrier waveforms for GNSS
In *2012 6th ESA Workshop on Satellite Navigation Technologies (Navitec 2012) & European Workshop on GNSS Signals and Signal Processing*, 2012, pp. 1–8.

[13] P. Dabove and V. Di Pietra
Towards high accuracy gnss real-time positioning with smartphones
Advances in Space Research, vol. 63, no. 1, pp. 94–102, 2019. [Online]. Available: https://www.sciencedirect.com/science/article/pii/S0273117718306537

[14] A. Nardin, F. Dovis, and J. A. Fraire
Empowering the tracking performance of LEO-based positioning by means of meta-signals
IEEE Journal of Radio Frequency Identification, vol. 5, no. 3, pp. 244–253, 2021.

[15] Z. Yao, J. Ma, J. Zhang, and M. Lu
Multicarrier Constant Envelope Composite Signal - A Solution to the Next Generation Satellite Navigation Signals
In *Proceedings of the 30th International Technical Meeting of the Satellite Division of The Institute of Navigation (ION GNSS+ 2017)*, Portland, Oregon, Nov. 2017, pp. 1520–1533. [Online]. Available: https://www.ion.org/publications/abstract.cfm?articleID=15372

[16] Z. Yao, F. Guo, J. Ma, and M. Lu
Orthogonality-Based Generalized Multicarrier Constant Envelope Multiplexing for DSSS Signals
IEEE Transactions on Aerospace and Electronic Systems, vol. 53, no. 4, pp. 1685–1698, Aug. 2017, number: 4. [Online]. Available: http://ieeexplore.ieee.org/document/7858582/

[17] P. Teunissen and O. Montenbruck
Springer handbook of global navigation satellite systems. Springer, 2017.

[18] R. Knight
ESA outlines plans for demo of LEO PNT satellites as part of FutureNAV, gives other updates
Inside GNSS, 2022, Accessed on: Dec. 31, 2022. [Online]. Available: https://insidegnss.com/esa-outlines-plans-for-demo-of-leo-pnt-satellites-as-part-of-futurenav-gives-other-updates/

[19] F. S. Prol *et al.*
Position, navigation, and timing (pnt) through low earth orbit (leo) satellites: A survey on current status, challenges, and opportunities
IEEE Access, vol. 10, pp. 83 971–84 002, 2022.

[20] T. G. Reid *et al.*
Satellite Navigation for the Age of Autonomy
In *2020 IEEE/ION Position, Location and Navigation Symposium (PLANS)*. Portland, OR, USA: IEEE, Apr. 2020, pp. 342–352. [Online]. Available: https://ieeexplore.ieee.org/document/9109938/

[21] F. van Diggelen
High-Sensitivity GNSS
In *Position, Navigation, and Timing Technologies in the 21st Century*. John Wiley & Sons, Ltd, 2020, pp. 445–479. [Online]. Available: http://onlinelibrary.wiley.com/doi/abs/10.1002/9781119458449.ch18

[22] A. Nardin, F. Dovis, and J. A. Fraire
Empowering the tracking performance of LEO PNT by means of meta-signals
In *2020 IEEE International Conference on Wireless for Space and Extreme Environments (WiSEE)*, 2020, pp. 153–158.

[23] Z. Yao and M. Lu
Next-Generation GNSS Signal Design. Springer, Singapore, 2021.

[24] E. Kaplan and C. Hegarty
Understanding GPS/GNSS: Principles and Applications. Artech House, 2017.

[25] C. Wang, X. Cui, T. Ma, S. Zhao, and M. Lu
Asymmetric Dual-Band Tracking Technique for Optimal Joint Processing of BDS B1I and B1C Signals
Sensors, vol. 17, no. 10, p. 2360, Oct. 2017, number: 10 Publisher: Multidisciplinary Digital Publishing Institute. [Online]. Available: https://www.mdpi.com/1424-8220/17/10/2360

[26] W. Zhang, Z. Yao, and M. Lu
WHAT: Wideband High-Accuracy Joint Tracking Technique for BDS B1 Composite Signal
In *2019 IEEE 9th International Conference on Electronics Information and Emergency Communication (ICEIEC)*, Jul. 2019, pp. 178–182, iSSN: 2377-844X.

[27] Y. Gao, Z. Yao, and M. Lu
High-precision unambiguous tracking technique for BDS B1 wideband composite signal
NAVIGATION, vol. 67, no. 3, pp. 633–650, 2020, _eprint: https://onlinelibrary.wiley.com/doi/pdf/10.1002/navi.377. [Online]. Available: https://onlinelibrary.wiley.com/doi/abs/10.1002/navi.377

[28] Z. Tian, X. Cui, G. Liu, and M. Lu
LPRA-DBT: Low-Processing-Rate Asymmetrical Dual-Band Tracking Method for BDS-3 B1I and B1C Composite Signal
In *Proceedings of the 2022 International Technical Meeting of The Institute of Navigation*, Jan. 2022, pp. 1027–1038, iSSN: 2330-3646.

[29] C. Wang, X. Cui, T. Ma, S. Zhao, and M. Lu
Asymmetric dual-band tracking technique for optimal joint processing of bds b1i and b1c signals
Sensors, vol. 17, no. 10, 2017. [Online]. Available: https://www.mdpi.com/1424-8220/17/10/2360

[30] J.-L. Issler, M. Paonni, and B. Eissfeller
Toward centimetric positioning thanks to L-and S-band GNSS and to meta-GNSS signals
In *2010 5th ESA Workshop on Satellite Navigation Technologies and European Workshop on GNSS Signals and Signal Processing (NAVITEC)*. IEEE, 2010, pp. 1–8.

[31] M. Paonni, J. Curran, M. Bavaro, and J. Fortuny
GNSS meta-signals: coherently composite processing of multiple GNSS signals
In *Proceedings of the 27th International Technical Meeting of The Satellite Division of the Institute of Navigation, Tampa, FL, USA*, 2014, pp. 8–12.

[32] P. Das, L. Ortega, J. Vilà-Valls, F. Vincent, E. Chaumette, and L. Davain
Performance limits of GNSS code-based precise positioning: GPS, Galileo & meta-signals
Sensors, vol. 20, no. 8, 2020. [Online]. Available: https://www.mdpi.com/1424-8220/20/8/2196

[33] L. Ortega, D. Medina, J. Vilà-Valls, F. Vincent, and E. Chaumette
Positioning Performance Limits of GNSS Meta-Signals and HO-BOC Signals
Sensors, vol. 20, no. 12, p. 3586, Jun. 2020, number: 12. [Online]. Available: https://www.mdpi.com/1424-8220/20/12/3586

[34] D. Borio and C. Gioia
Reconstructing gnss meta-signal observations using sideband measurements
NAVIGATION: Journal of the Institute of Navigation, vol. 70, no. 1, 2023. [Online]. Available: https://navi.ion.org/content/70/1/navi.558

[35] D. Borio
Hypercomplex Representation and Processing of GNSS Signals
In *Proceedings of the 35th International Technical Meeting of the Satellite Division of The Institute of Navigation (ION GNSS+ 2022)*, Sep. 2022, pp. 3160–3179, iSSN: 2331-5954.

[36] M. S. Hameed, T. Woerz, T. Pany, J. Wendel, M. Paonni, and T. Senni
Demonstration of Meta-signal Positioning using LAMBDA Ambiguity Fixing Method within a Bit-true Simulation
In *Proceedings of the 34th International Technical Meeting of the Satellite Division of The Institute of Navigation (ION GNSS+ 2021)*, Sep. 2021, pp. 2819–2837, iSSN: 2331-5954.

[37] J. Garcia-Molina
Unambiguous Meta-Signal Processing: A Path to Code-Based High-Accuracy PNT (InsideGNSS, March/April 2021)
Inside GNSS, Mar. 2021.

[38] C. Schwalm, C. Enneking, and S. Thoelert
Ziv-Zakai Bound and Multicorrelator Compression for a Galileo E1 Meta-Signal
In *2020 European Navigation Conference (ENC)*, Nov. 2020, pp. 1–9.

[39] European Union
European GNSS (galileo) open service, signal-in-space interface control document (OS SIS ICD V2.0)
January 2021. [Online]. Available: https://www.gsc-europa.eu/sites/default/files/sites/all/files/Galileo_OS_SIS_ICD_v2.0.pdf

[40] T. Reid
Opportunities in Commercial LEO Satellite Navigation
In *Proceedings of the 34th International Technical Meeting of the Satellite Division of The Institute of Navigation (ION GNSS+ 2021)*, Sep. 2021, pp. 2012–2048, iSSN: 2331-5954. [Online]. Available: http://www.ion.org/publications/abstract.cfm?jp=p&articleID=18106

[41] P. A. Iannucci and T. E. Humphreys
Economical fused LEO GNSS
In *2020 IEEE/ION Position, Location and Navigation Symposium (PLANS)*, 2020, pp. 426–443.

[42] A. Nardin, F. Dovis, and B. Motella
Impact of non-idealities on GNSS meta-signals processing
In *Proceedings European Navigation Conference (ENC) 2020*, Dresden, Nov. 2020.

[43] R. McDonough and A. Whalen
Detection of Signals in Noise. Amsterdam: Elsevier Inc., 1995, pp. 383–445.

[44] J. W. Betz and K. R. Kolodziejski
Generalized Theory of Code Tracking with an Early-Late Discriminator Part I: Lower Bound and Coherent Processing

IEEE Transactions on Aerospace and Electronic Systems, vol. 45, no. 4, pp. 1538–1556, Oct. 2009, number: 4. [Online]. Available: https://ieeexplore.ieee.org/document/5310316/

[45] J. W. Betz
The offset carrier modulation for GPS modernization
In *Proceedings of the 1999 National Technical Meeting of The Institute of Navigation*, San Diego, CA, 1999, pp. 639–648.

[46] A. Nardin
Innovative signal processing solutions for next-generation satellite navigation systems
Ph.D. dissertation, Politecnico di Torino, 2023.

[47] A. Weiss and E. Weinstein
Fundamental limitations in passive time delay estimation–Part I: Narrow-band systems
IEEE Transactions on Acoustics, Speech, and Signal Processing, vol. 31, no. 2, pp. 472–486, Apr. 1983, conference Name: IEEE Transactions on Acoustics, Speech, and Signal Processing.

[48] E. Weinstein and A. Weiss
Fundamental limitations in passive time-delay estimation–Part II: Wide-band systems
IEEE Transactions on Acoustics, Speech, and Signal Processing, vol. 32, no. 5, pp. 1064–1078, Oct. 1984, conference Name: IEEE Transactions on Acoustics, Speech, and Signal Processing.

[49] J. Wendel, F. M. Schubert, and S. Hager
A robust technique for unambiguous boc tracking
NAVIGATION, vol. 61, no. 3, pp. 179–190, 2014.

[50] Z. Yao, Y. Gao, Y. Gao, and M. Lu
Generalized theory of boc signal unambiguous tracking with two-dimensional loops
IEEE Transactions on Aerospace and Electronic Systems, vol. 53, no. 6, pp. 3056–3069, 2017.

[51] J. J. Spilker Jr, P. Axelrad, B. W. Parkinson, and P. Enge
Global Positioning System: Theory and Applications, Volume I. American Institute of Aeronautics and Astronautics, 1996.

[52] Z. M. Kassas *et al.*
Navigation with multi-constellation leo satellite signals of opportunity: Starlink, oneweb, orbcomm, and iridium
In *2023 IEEE/ION Position, Location and Navigation Symposium (PLANS)*, 2023, pp. 338–343.

[53] M. Su, X. Su, Q. Zhao, and J. Liu
Beidou augmented navigation from low earth orbit satellites
Sensors, vol. 19, no. 1, 2019. [Online]. Available: https://www.mdpi.com/1424-8220/19/1/198

[54] I. del Portillo, B. G. Cameron, and E. F. Crawley
A technical comparison of three low earth orbit satellite constellation systems to provide global broadband
Acta Astronautica, vol. 159, pp. 123–135, 2019. [Online]. Available: https://www.sciencedirect.com/science/article/pii/S0094576518320368

[55] E. Kaplan and C. Hegarty
Understanding GPS: principles and applications. Artech house, 2005.

[56] B. Chen and C. Tong
Radar multipath scattering from the composite model: Specular image modified model and isar imaging analysis
International Journal of RF and Microwave Computer-Aided Engineering, vol. 29, no. 12, p. e21956, 2019. [Online]. Available: https://onlinelibrary.wiley.com/doi/abs/10.1002/mmce.21956

[57] R. U. R. Lighari, M. Berg, J. Kallankari, A. Parssinen, and E. T. Salonen
Analysis of the measured rhcp and lhcp gnss signals in multipath environment
In *2016 International Conference on Localization and GNSS (ICL-GNSS)*, 2016, pp. 1–6.

Andrea Nardin (GS'20) received the M.Sc. degree in telecommunications engineering in 2018 and the Ph.D. in electrical, electronics and communications engineering in 2023, both from Politecnico di Torino, Turin, Italy, where he is currently a postdoctoral researcher with the Department of Electronics and Telecommunications. From 2018, he has been working with the Navigation Signal Analysis and Simulation (NavSAS) group at Politecnico di Torino and in 2021 he was a Visiting Doctoral Researcher at Northeastern University, Boston, MA, USA with the center for Signal Processing, Imaging, Reasoning, and Learning (SPIRAL). His research interests include signal processing architectures and signal design applied to GNSSs and LEO PNT.

Fabio Dovis (GS'98-M'01) was born in Bruino, Italy,in 1970. He received his M.Sc. degree in 1996 and his Ph.D. degree in 2000, both from Politecnico di Torino, Turin, Italy. He joined the Department of Electronics and Telecommunications of Politecnico di Torino as an assistant professor in 2004 and as associate professor in 2014. Since 2021 he is a full professor in the same department where he coordinates the Navigation Signal Analysis and Simulation (NavSAS) research group. He has a relevant experience in European projects in satellite navigation as well as cooperation with industries and research institutions. He serves as a member of the IEEE Aerospace and Electronics Systems Society Navigation Systems Panel. His research interests cover the design of GPS and Galileo receivers and advanced signal processing for interference and multipath detection and mitigation, as well as ionospheric monitoring.

Francesca Zanier received the M.Sc. degree in telecommunications engineering and the Ph.D. degree from the University of Pisa, Italy. She joined the European Space Agency, ESTEC, Noordwijk, The Netherlands, in 2009, where she is currently a Radio Navigation System Engineer with the Radio Navigation Systems and Techniques Section of the Technical Directorate. Her research interests include signal processing, estimation theory, GNSS receivers, and signals and navigation applications.

Floor Melman received his master degree in Aerospace Engineering in 2018 from the Delft University of Technology (TU Delft). From December 2018 to August 2020, he worked as a Young Graduate Trainee (YGT) in the navigation directorate on Galileo signals and receivers. Since 2020, he works as a Radio Navigation Engineer at ESA/ESTEC. His main areas of work include PNT algorithms (in harsh environments) and GNSS signal processing.